Published in final edited form as:

Nano Today. 2013 December 1; 8(6): 566–576. doi:10.1016/j.nantod.2013.11.001.

A computational framework for identifying design guidelines to increase the penetration of targeted nanoparticles into tumors

Sabine Hauert[a], **Spring Berman**[b], **Radhika Nagpal**[c], and **Sangeeta N. Bhatia**[a,d,e,f]

Sabine Hauert: shauert@mit.edu; Spring Berman: spring.berman@asu.edu; Radhika Nagpal: rad@eecs.harvard.edu; Sangeeta N. Bhatia: sbhatia@mit.edu

[a]Harvard-MIT Division of Health Sciences and Technology, Massachusetts Institute of Technology, Cambridge, MA 02139, USA

[b]Mechanical and Aerospace Engineering, Arizona State University, Tempe, AZ 85287, USA

[c]Computer Science, Harvard University, Cambridge, MA 02138, USA

[d]Department of Electrical Engineering and Computer Science, Massachusetts Institute of Technology, Cambridge, MA 02139, USA

[e]Division of Medicine, Brigham and Women's Hospital, Boston, MA 02115, USA

[f]Howard Hughes Medical Institute, Massachusetts Institute of Technology, Cambridge, MA 02139, USA

Abstract

Targeted nanoparticles are increasingly being engineered for the treatment of cancer. By design, they can passively accumulate in tumors, selectively bind to targets in their environment, and deliver localized treatments. However, the penetration of targeted nanoparticles deep into tissue can be hindered by their slow diffusion and a high binding affinity. As a result, they often localize to areas around the vessels from which they extravasate, never reaching the deep-seeded tumor cells, thereby limiting their efficacy. To increase tissue penetration and cellular accumulation, we propose generalizable guidelines for nanoparticle design and validate them using two different computer models that capture the potency, motion, binding kinetics, and cellular internalization of targeted nanoparticles in a section of tumor tissue. One strategy that emerged from the models was delaying nanoparticle binding until after the nanoparticles have had time to diffuse deep into the tissue. Results show that nanoparticles that are designed according to these guidelines do not require fine-tuning of their kinetics or size and can be administered in lower doses than classical targeted nanoparticles for a desired tissue penetration in a large variety of tumor scenarios. In the future, similar models could serve as a testbed to explore engineered tissue-distributions that arise when large numbers of nanoparticles interact in a tumor environment.

Corresponding Author: Sangeeta Bhatia, Massachusetts Institute of Technology, 77 Massachusetts Ave. Bldg. 76-453, Cambridge, MA 02139, USA, sbhatia@mit.edu, +1 617 324 0610.

Keywords

Targeting; Nanoparticle; Modeling; Tissue Penetration; Cancer; Systems Nanotechnology

1. Introduction

Nanoparticles targeted to surface receptors that are over-expressed in certain tumors have the potential to improve specificity and intracellular delivery of therapeutic payloads to cancer cells [1]. Their size, typically in the 5–200 nm range, enables them to leak out of angiogenic vessels and accumulate in tumors [2]. Once in the tumor tissue, nanoparticles must traverse the interstitial space to reach all cells that require treatment [3]. This is a challenging goal because high, uniform pressure in tumor environments causes nanoparticle motion to be mostly diffusive [4, 5]. In addition, nanoparticles with large binding affinities, amplified by multivalent interactions, will accumulate in the first cells they encounter after extravasation as depicted in Fig. 1A. The resulting binding-site barriers, previously demonstrated with antibodies [6] and recently with targeted nanoparticles [7, 8], prevent treatments from reaching cells far away from vessels.

Efforts have been made to overcome transport barriers that limit the accumulation of nanoparticles in tumor tissue [4]. Solutions include increasing nanoparticle circulation time [9], or activating transvascular transport, and parenchyma penetration through the use of tumor-penetrating peptides [10, 11].[1] Rather than approach nanoparticle design empirically, models by Thurber et al. [6, 12] and Wittrup et al. [13] are able to quantitatively predict the impact of dosage, blood flow, extravasation, diffusion, and binding kinetics on the distribution of antibodies and macromolecules in tumors. Other models by Ferrari et al. [14] focus on the targeting of nanoparticles to the vasculature. To date, most models have been used to investigate how existing nanoparticle designs impact tissue distribution; the next step is to implement computational models that drive innovation by helping to explore novel nanoparticle designs and offer the potential to yield generalizable guidelines for a variety of tumor scenarios. Furthermore, current models do not consider the ability of targeted nanoparticles to accumulate at effective doses in individual cancer cells given a specific therapeutic cargo. Finally, researchers typically rely on deterministic models that assume nanoparticles can be modeled as populations that are not subject to stochastic variations.

Using a deterministic model, which is further validated by stochastic simulations, we systematically explore nanoparticle designs that result in binding-site barriers and propose generalizable guidelines to avoid such barriers without increasing the injected dose or fine-tuning nanoparticle diffusion coefficients and binding kinetics. Rather than consider all transport parameters that impact nanoparticle distribution, we model a challenging representative tumor scenario in which a defined low number of targeted nanoparticles must accumulate to kill individual receptor-rich cells, including those located furthest from the tumor vasculature. Results show that many targeted nanoparticle designs reported in the literature lead to superficial tumor penetration in this scenario. The therapeutic payload is

[1]See our video on nanoparticle transport in tumors: http://youtu.be/gBYkYzj7CKM

taken into account in calculating the number of nanoparticles needed to affect tumor cells. Optimization of the deterministic model shows that overcoming the barrier would typically require large treatment doses to saturate cells near tumor vessels before nanoparticles can penetrate deeper into the tissue. Rather than fine-tune the size and binding affinity of nanoparticles to improve tissue penetration, we augment our models to explore novel design guidelines that rely on delaying nanoparticle binding until after the nanoparticles have had time to diffuse deep into the tissue. Results in simulation show that nanoparticles designed following these guidelines can accumulate at effective levels in all cells that require treatment with the use of smaller injected doses than would be necessary for conventional targeted nanoparticles. The design guidelines are immediately generalizable to a variety of tumor scenarios that account for variations in surface receptor expression and recycling, drug encapsulation, number of nanoparticles, and the rate at which nanoparticles accumulate in the tumor tissue. Furthermore, we outline existing, established technologies that could be used to implement these guidelines in reality. Beyond deep tissue penetration, we aim to ultimately control the distribution of nanoparticles in tissue with sufficient precision to accommodate heterogeneous treatment and imaging needs. To this end, we propose the use of nanoparticles with targeting moieties whose unveiling is a function of an environmental stimulus rather than time or external triggers. Using this strategy, we demonstrate in simulation that the nanoparticles could achieve inverted internalization gradients by accumulating more in cells further away from the vasculature. Such a distribution pattern could be useful to deliver drugs deep into tumors.

2. Materials and methods

2.1 In Silico Models

Computer simulations can help engineer nanotreatments by rapidly predicting experimental outcomes for a large set of design parameters. To this end, we formulate both deterministic and stochastic reaction-diffusion models to simulate the transport, binding kinetics, and internalization of nanoparticles in a section of tumor tissue.

The main challenge is to back out usable guidelines that generalize across tumor scenarios and can therefore be implemented in reality. Varying all the parameters that impact nanoparticle transport is unrealistic and typically results in a variety of regimes and tradeoffs that are difficult to translate to actionable guidelines. Instead, we focus on a representative scenario, which embodies a challenging tumor environment that would realistically be encountered by targeted nanoparticles. Solutions to this scenario have the potential to automatically generalize to many tumor environments. Our focus is on scenarios that result in binding-site barriers. Specifically, we consider the situation depicted in Fig. 1B in which nanoparticles leaving a vessel near the central, poorly perfused area of the tumor need to penetrate deep into the tumor tissue up to a depth L, while accumulating at levels sufficient to kill each of the N cells along the way. Each cell is represented as a cubic region that has a volume of S^3, where S is the largest cell dimension. The percent injected dose (PID) of drugs with high potency P reaching the tumor section is sufficient to theoretically kill or treat (e.g. through siRNA delivery) all cells if distributed uniformly throughout the tissue. The PID is measured at a predefined time T after the nanoparticle injection. Based on the

weight *W* of a mouse and the ratio of the entire tumor volume V_T to the volume of the simulated tumor section $S^2 L$, we can approximate the minimal injected dose (*ID*) of drugs in mass per body weight needed to accumulate at *PID* levels at time *T* after injection. Each nanoparticle encapsulates a large number *E* of drug molecules with molar mass *M*, resulting in a low number NP_0 of nanoparticles that are present in the simulated tumor section for the predefined injected dose of drug. To approximate a slow clearance of the nanoparticles from the blood, the model is initialized with NP_0 nanoparticles that enter the first cell region of the tumor tissue section at a uniform rate over the duration of the circulation time T_C. Nanoparticles diffuse through the tumor tissue and bind to highly expressed receptors [15] that are immediately recycled upon internalization of the nanoparticles. We can approximate NP_0 as

$$NP_0 = ID \cdot W \cdot \frac{PID \cdot S^2 \cdot L}{V_T} \cdot \frac{N_A}{M \cdot E}, \quad \text{Eq. 1}$$

where N_A is the Avogadro constant.

The reaction-diffusion model illustrated in Fig. 1C describes the formation and dissociation of nanoparticle-receptor complexes and the internalization of nanoparticles in each cell of the tumor model [16]. The species in the reaction network are defined as NP_F, free nanoparticles; NP_I, internalized nanoparticles; *R*, receptors; and *C*, nanoparticle-receptor complexes. Free nanoparticles diffuse between cell regions with diffusion coefficient *D*. The reaction network is:

$$NP_F + R \underset{}{\overset{k_a, k_d}{\longleftrightarrow}} C \xrightarrow{k_i} NP_I + R \quad \text{Eq. 2}$$

where k_a and k_d are the association and dissociation rate constants and k_i is the internalization rate constant.

Both the stochastic and deterministic models proposed here describe the population dynamics of nanoparticles in tumors, and thus are less computationally expensive than simulations of the movement of individual nanoparticles and their interactions with other nanoparticles or receptors. The stochastic model has a more legitimate physical basis than the deterministic model: it captures fluctuations and correlations in population levels that occur in reaction-diffusion systems, and it realistically represents these populations as integers that change by discrete amounts [13]. The deterministic formulation is accurate for systems with large populations whose fluctuations remain small relative to the absolute population levels. This model represents the system state as concentration fields that evolve continuously according to partial differential equations. The dimensionality of the deterministic model is independent of the population levels, and for large populations it is faster to numerically solve this model than to simulate the stochastic model. Hence, when accurate, the deterministic model is more suitable as a tool for quickly predicting the system behavior for a large set of parameters. In this paper, we use deterministic models to simulate all experiments and validate key results using a stochastic simulator.

2.2 Deterministic Model

The deterministic model of the system consists of a set of reaction-diffusion partial differential equations (PDEs) that govern the expected spatiotemporal evolution of the different species populations in the one-dimensional domain of interest. The population levels of free nanoparticles, $NP_F(x,t)$, internalized nanoparticles, $NP_I(x,t)$, receptors, $R(x,t)$, and nanoparticle-receptor complexes, $C(x,t)$, are defined at each position $x \in [0\ L]$ at each time $t \geq 0$ and are expressed in units [number/cell]. The equations for the PDE model are:

$$\begin{aligned}\frac{\partial NP_F}{\partial t} &= D \cdot \nabla^2 \cdot NP_F - k_a \cdot NP_F \cdot R + k_d \cdot C \\ \frac{\partial R}{\partial t} &= -k_a \cdot NP_F \cdot R + k_d \cdot C + k_i \cdot C \\ \frac{\partial C}{\partial t} &= k_a \cdot NP_F \cdot R - k_d \cdot C - k_i \cdot C \\ \frac{\partial NP_I}{\partial t} &= k_i \cdot C.\end{aligned}$$

NP_0 represents a direct measure of the number of nanoparticles present in the simulated tumor section after extravasation and clearance at time T. Focus is on modeling where these nanoparticles distribute within the simulated tumor tissue. Initially, no nanoparticles are present in the domain, and N_R receptors are distributed uniformly throughout each of the cells. The model boundary condition at $x = 0$ is defined as a constant-rate extravasation of the NP_0 free nanoparticles into the first cell region over time period T_C. Due to the local symmetry of the tumor environment at the micro-scale, we assume that nanoparticles that diffuse out of the tumor section at $x = L$ are replaced by nanoparticles flowing in from adjacent tissue. Hence, a Neumann boundary condition is applied at $x = L$:

$$\frac{\partial NP_F}{\partial t}(x,t)\Big|_{x=L} = 0, \quad t > 0.$$

The deterministic model is numerically integrated in MATLAB (Mathworks) using a finite difference method with 20 or more uniformly spaced nodes.

2.3 Stochastic Model

The stochastic model of the system takes the form of a Reaction-Diffusion (or Multivariate) Master Equation [17, 18]. In this model, the spatial domain is discretized into cubic subvolumes that are chosen small enough to be approximated as well-mixed regions [19]. The populations of different species in each subvolume change when chemical reactions occur inside the subvolume or when nanoparticles diffuse into or out of the subvolume. A stochastic simulation algorithm can be used to compute numerical realizations of the species populations over time in a way that takes into account the fact that these populations are integer-valued and exhibit randomness in their time evolution [20]. Various spatial stochastic simulators for reaction-diffusion systems have been developed in recent years [21]. We implement a stochastic simulator that is based on the freely available Stochastic Simulator Compiler (SSC) [22][2]. Briefly, for each cell region, the simulator determines how probable a reaction is compared to other reactions and when the next reaction should occur.

[2]Stochastic Simulator Compiler: http://web.mit.edu/irc/ssc/.

Based on the reaction network described in Eq. 2, associations happen with probability $k_a \cdot NP_F \cdot R$ per unit time, dissociations with probability $k_d \cdot C$ per unit time, and internalizations with probability $k_i \cdot C$ per unit time. Diffusion is modeled as a reaction in which a free nanoparticle jumps between neighboring cell regions with rate constant D/S^2; this occurrence happens with probability $2\ NP_F \cdot D/S^2$ per unit time. The next reaction should therefore happen after an exponentially distributed random time with mean $1/(k_a \cdot NP_F \cdot R + k_d \cdot C + k_i \cdot C + 2\ NP_F \cdot D/S^2)$ seconds and should randomly be chosen proportionally to the probability rate at which each reaction happens. After each reaction, the species populations and reaction probability rates are updated.

3. Results

3.1 Binding-Site Barriers

Providing guidelines for the improvement of nanoparticle design requires an understanding of which design parameters result in binding-site barriers. We focus on exploring parameters that have a direct effect on the distribution of nanoparticles in tissue after extravasation and can be modified through engineering. For example, diffusion coefficients can be modified by changing the size of nanoparticles [23, 24] or by relaxing the extracellular matrix [4], while binding kinetics can be modified by acting on multivalency and engineering targeting ligands [25]. Toward this end, we identified a relevant range of nanoparticle radii r and dissociation constants, defined as $K_D = k_d/k_a$, from the literature (Table 1).

Diffusion coefficients D were determined using the Stokes-Einstein equation [33] based on nanoparticle radii ranging from 2 nm to 500 nm and viscosities ranging from values for water to values for tumor tissue (10-fold increase in viscosity [4]). We simulated the effect of combinations of D and K_D in a representative challenging tumor scenario in which liposomes carrying high loads of a cytotoxic drug doxorubicin (e.g. Doxil) are targeted to over-expressed receptors [34] such as folate on KB cells [25] or HER-2 in certain breast cancer lines [35]. The values of the parameters for the scenario are given in Table 2.

Particles are required to penetrate at least L = 200 μm into the tissue [4], targeting 20 cells along the way. Only 1% of the injected dose reaches the tumor, which is typically the lower bound in tumor tissue accumulation for targeted nanoparticles [13, 36–38]. The *PID* is measured after T = 48 hours to ensure that the nanoparticles are able to diffuse far away from the vasculature. The number of internalized nanoparticles estimated to theoretically induce cytotoxicity in a single cell was calculated to be 600 using the equation $NP_c = (P \cdot S^3 \cdot N_A)/E$, where N_A is the Avogadro constant. Setting $NP_0 = 20\ NP_c$ in Eq. 1 corresponds to a local concentration of 10uM in all 20 cell regions of the scenario, which is the IC90 of doxorubicin. An injected dose ID = 3.3 mg/kg of doxorubicin is computed to be sufficient to kill all 20 cells if the nanoparticles distribute uniformly along the linear section of tumor in the model. However, to increase the likelihood that sufficient numbers of nanoparticles reach all cells, we administer a dose of 33 mg/kg, 10 times in excess of the theoretically sufficient dose. This corresponds to an initial nanoparticle population in the tumor model of $NP_0 = 1.2044 \cdot 10^5$, corresponding to a maximum concentration of 200 nM (for the nanoparticles) or 2 mM of doxorubicin in a cell region. As a reference, the typical

injected dose for liposomal doxorubicin in humans ranges from 20 mg/m^2 to 70 mg/m^2 [39], corresponding to a mouse equivalent range between 6.6 mg/kg and 25 mg/kg [40]. Doses up to 55 mg/kg have been shown to cause reversible weight loss in mice [41].

Fig. 2A shows the number of cells that are dead after 48 hours of treatment as a function of D and K_D, simulated using both the stochastic model and the deterministic model. Note that the identical results from both models validate the use of the deterministic model for prediction and optimization. Based on experimental work by Hong et al. [6, 25] and Thurber et al. [6], we maintained the dissociation and internalization rate constants at $k_d = 10^{-4}\ s^{-1}$, $k_i = 10^{-5}\ s^{-1}$ while varying k_a in the range $[10^3, 10^9]\ M^{-1}s^{-1}$. These are the parameter ranges used throughout the paper, unless stated otherwise. Fig. 2B shows the penetration profiles of several nanoparticle formulations. As further validation, previous models by Thurber et al. [6] for antibody penetration showed that treatments with $D = 3 \cdot 10^{-7}\ cm^2/s$ and $K_D = 8$ nM were able to penetrate a depth of at least 200 μm into tumor tissue while antibodies with $K_D = 30$ pM were not, which is consistent with findings presented here. The results show that most of the nanoparticle formulations considered are not capable of killing all 20 cells in the model. Nanoparticles with a high binding affinity (Fig. 2B(a),(c)), regardless of their speed, accumulate only in cells near the vasculature, and slow nanoparticles (Fig. 2B(c,d)) fail to accumulate at lethal levels in cells farthest from the vasculature. Fast nanoparticles with a low binding affinity are able to accumulate at lethal levels in all cells (Fig. 2B(b)).

However, lowering the affinity beyond the range explored here could result in nanoparticles that are unable to accumulate at lethal levels in tumor cells. Simulations show this to be true for nanoparticles with dissociations constants in the micro-molar range. For the remaining formulations, a balance between nanoparticle speed and binding affinity is required to treat cells throughout the entire tumor section. Other studies have suggested that multivalency mostly affects the dissociation rate rather than the association rate [42]. In Fig. 2C we show that maintaining $k_a = 10^4\ M^{-1}s^{-1}$ constant and varying k_d in the range $[10^{-6},1]\ s^{-1}$ yields similar results. Overall, many of the targeted nanoparticle formulations in the literature would result in binding-site barriers in the scenario proposed here (Fig. 2D and Table 1). To overcome this barrier, nanoparticles would require a reduction in size to produce a higher diffusion coefficient or a fine-tuning of their binding affinity. For liposomes, size variation can be achieved by choosing the appropriate extrusion membrane [43]. Reducing the valency of the targeting ligand or engineering the ligand itself can reduce affinity [25, 44]. For many nanoparticles formulations however, size and affinity manipulations are time-consuming and detrimental to nanoparticle function [45].

The common solution to overcome binding-site barriers is to increase the injected dose, ID. Saturating the first cells after extravasation could enable excess nanoparticles to overcome the barrier and penetrate deeper into the tissue. To test this hypothesis in simulation, we determined the minimum injected dose needed for each of the 20 cells to accumulate sufficient internalized nanoparticles to kill an individual cell, NP_c, for each parameter set (K_D, D). Using branch and bound optimization, we computed this minimum injected dose as the value in the range $[ID_{min}, ID_{max}] = [0, 33000]$ mg/kg that maximizes the following function:

$$f(ID)=\begin{cases} 1-\frac{ID-ID_{\min}}{ID_{\max}-ID_{\min}} & \text{if all cells are dead after 48 h} \\ 0 & \text{otherwise.} \end{cases}$$

Cell death was predicted from the deterministic model, which was initialized with the free nanoparticle population NP_0 that corresponds to the computed *ID* according to Eq. 1. As shown in Fig. 2E, 400-fold increases in dose from 33 mg/kg would be required to overcome binding-site barriers for several nanoparticle formulations, leading to systemic toxicity for the treated mice [41].

3.2 Time-Dependent Binding

Rather than increase the injected dose or fine-tune nanoparticle formulations, we propose a generalizable solution to achieve targeted deep tissue penetration with a broad range of nanoparticle designs. We consider a strategy in which nanoparticles are initially prevented from binding while diffusing through tumor tissue. The nanoparticle binding functionality is then restored as a function of time or an external human-operated trigger such as light, heat, magnetic fields, or injected chemicals (Fig. 3A) [46]. In the simplest form of this implementation, nanoparticles would be prevented from binding for a duration T_{delay} before entirely regaining their original binding capabilities. This scenario is modeled by setting the association rate constant to zero until time T_{delay} and to k_a thereafter according to a step function. For each parameter set (K_D, D), we determined the minimum values of T_{delay} that lead to the accumulation of a lethal dose of internalized nanoparticles in each cell. Using line-search optimization, we computed the minimum T_{delay} as the value in the range [0, T_{max}] = [0, 48] h that maximizes the following function:

$$f(T_{delay})=\begin{cases} 1-T_{delay}/T_{\max} & \text{if all cells are dead after 48 h} \\ 0 & \text{otherwise.} \end{cases}$$

The minimum T_{delay} values that lead to the death of all target cells for each parameter set (K_D, D) are given in Fig. 3B. Fast-diffusing nanoparticles with $D = 10^{-6}$, 10^{-7}, 10^{-8} cm^2/s can unveil their binding-moieties as early as T_{delay} = 3h00, 3h20, 4h55 after injection to result in full tissue penetration and target cell death. Slower-diffusing nanoparticles with $D = 10^{-9}$ cm^2/s should wait at least 17h15 as shown in Fig. 3C. A single binding delay of 17h15 therefore has the potential to enable all nanoparticle formulations to overcome binding-site barriers in our simulated scenario without increasing the injected dose. While most nanoparticle formulations are retained in the tumor environment due to the enhanced permeability and retention effect [4, 43], small nanoparticles that are prevented from binding for too long risk diffusing to the rim of the tumor where the pressure difference between the tumor and the surrounding tissue will irreversibly drive them out of the tumor [5, 8, 47]. As a reference, it would take the fastest-diffusing nanoparticles in our model approximately 34 hours to diffuse from the center of the simulated tumor to its rim. If fast tissue clearance is a concern, bioengineers can implement two binding delay regimes of 4h55 for fast nanoparticles ($D = 10^{-6}$, 10^{-7}, 10^{-8} cm^2/s) and 17h15 for slow nanoparticles. Another concern is non-specific uptake of veiled nanoparticles by macrophages present in the tumor

environment that could prevent their diffusion deep into the tissue. Based on research by Thurber et al. [48], we estimate the rate of non-specific cellular uptake by macrophages to be slow relative to diffusion, even for the smallest diffusion coefficient of 10^{-9} cm^2/s considered here.

The representative scenario used to design these guidelines was chosen to be challenging. By relaxing the different parameters of the scenario, we show that the delayed binding strategy can directly be generalized to a large variety of tumor environments without modification. In particular, we consider scenarios where the cell receptors are not recycled, the number of cell receptors is reduced ($R = 10^5$), the *PID* of nanoparticles reaching the tumor is increased (*PID* = 10%), nanoparticles accumulate immediately in the tumor section ($T_c = 0$), and nanoparticles are loaded with lower amounts of drug ($E = 10^3$). The number of cells killed for each parameter set (K_D, D), as predicted by the deterministic model with no binding delay and *ID* = 33 mg/kg, is plotted in Fig. 3D. The figure shows that while these scenarios should intuitively reduce the prevalence of binding-site barriers, the majority of nanoparticle formulations still result in poor tissue penetration and cellular accumulation. Fig. 3E shows that delaying the binding by 17h15, as suggested by our guidelines, results in complete cell death in all scenarios considered. We further tested the impact of slow drug release by nanoparticles implementing the delayed binding strategy. Results show that nanoparticles that are only able to deliver 30% of their cargo within 48 hours are still able to kill all cells for formulations with fast diffusion ($D = 10^{-6}$, 10^{-7}, 10^{-8} cm^2/s) while killing half of the cells when the diffusion is slow ($D = 10^{-9}$ cm^2/s).

3.3 Space-Dependent Binding

Beyond targeted deep tissue penetration, we aim to ultimately control the spatial distribution of nanoparticles in tissue. In our simulations, more nanoparticles internalized in cells located near the vasculature than in cells present at deeper sites in the tissue. Inverting this gradient, *i.e.*, achieving low amounts of internalized nanoparticles near the vasculature and high amounts deep in the tissue, could be beneficial to deliver large doses of drugs deep into tumors. To produce this inverted gradient, the unveiling of binding-moieties should rely on local, spatially-dependent signals in the environment rather than on a global external signal (time- or human-triggered). In the simplest case, nanoparticles can react to natural gradients in the tumor environment based on pH or enzymatic activity [7, 49–55]. To account for the impact of the environment, we introduce a new species in our reaction-diffusion system called *unveilers*, represented with the symbol U, and a species of veiled freely diffusing nanoparticles denoted by NP_V. Unveilers are abstractions for elements that could be used as triggers for unveiling binding moieties. As an example, we consider a scenario where the population level of unveilers, $U(x,t)$, is initially distributed in the tumor model according to $U(x,0) = cx$, where c is an arbitrary constant and x is the distance from the vessel. We then add a reaction to the network described in Eq. 2 in which a veiled nanoparticle NP_V that encounters an unveiler U will become an unveiled nanoparticle NP_F at rate constant k_u. Fig. 4 shows a tissue penetration profile computed by the stochastic simulator for the original test-case scenario with $c = 5\cdot 10^7$, $D = 10^{-8}$ cm^2/s, $K_D = 0.01$ nM, $k_u = 6\cdot 10^2$ M^{-1}s^{-1}, and *ID* = 33 mg/kg. Without unveilers, these parameter values result in a binding-site barrier, as shown in Fig. 2A. As illustrated in Fig. 4, the unveilers cause nanoparticles to internalize

most in cells located far from the vasculature, producing an inverted internalization gradient and killing cells deep in the tumor tissue. In the future, a better understanding of the tumor environment and the binding kinetics of nanoparticles could lead to increased control over nanoparticle distribution in tumor tissue. This level of control could be useful to create nanoparticle-based beacon systems or maps that point out areas of interest in the body or produce communication signals that can be sensed by other nanoparticles [56].

4. Discussion

Using computational frameworks, we are able to provide generalizable guidelines for the design of novel targeted nanoparticles that can accumulate in cells located deep in tumors. Building on these guidelines, the next step is to engineer nanoparticles in reality with the identified features. Bioengineers have already designed and constructed a number of nanoparticles that are able to shield targeting moieties, or non-specific cellular uptake mechanisms mediated by charge or cell penetrating peptides (CPP), as a function of protease activity or pH levels in tumor environments [8, 49]. Interestingly, most of these nanoparticles were intended to increase the macroscopic accumulation of nanoparticles in tumors as opposed to healthy tissue [50, 52, 57–61]. Results reported here suggest that repurposing these shielding mechanisms could result in a generalizable strategy to improve micro-scale distributions of nanoparticles within the tumor tissue itself. In particular, nanoparticles engineered by Harris et al. [52] are able to unveil most targeting moieties in tumor environments within 24 hours based on enzymatic activity and have shown increased tumor penetration as a result. In a similar fashion, MMP-activatable cell-penetrating peptides were shown to penetrate well beyond the blood vessels from which they extravasate [57, 59]. Layer-by-layer nanoparticles described by Poon et al. [50] are able to unveil a positively charged nanoparticle surface as a function of pH within the tumor environment, with 50% of the unveiling happening within 3 to 4 hours in the tumor. pH titratable iron oxide nanoparticles produced by Crayton et al. are able to accumulate in acidic tumor microenvironments by changing from neutral to positively charged [60]. Romberg et al. review the different mechanisms that can be used to shed nanoparticle PEG coatings to improve drug release and cellular uptake while increasing circulation time [61]. Lee et al. propose a remote optical switch for the spatial and temporal control of nanoparticle functionalities [62]. Finally, work by Partlow et al. [63] suggests that lipid raft transport with membrane targeted nanoparticles could enable targeted delivery of lipophilic substances without the need for entire nanoparticle internalization, thereby improving the ability of nanoparticles to penetrate deep in tissue. Overall, these advances in nanoparticle engineering are strong indications that the design guidelines identified here can be translated to working systems in reality.

5. Conclusions

Nanoparticles targeted to cancer cells are designed to specifically deliver treatment cargos. While they are able to passively accumulate in tumor tissue through the enhanced permeability and retention effect [4], targeted nanoparticles often internalize in the first cells they encounter after extravasation. Indeed, the diffusive nature of certain tumor environments and the strong binding affinity of many nanoparticles in the literature result in

the development of binding-site barriers. Overcoming these barriers would require large doses of nanoparticles that could lead to systemic toxicity [41]. Instead, we propose novel generalizable guidelines that enable a non-toxic dose of nanoparticles to achieve full tissue penetration and accumulate at effective levels in all target cells. The strategy is to delay binding until after nanoparticles have had time to diffuse deep into the tissue. By applying optimization techniques to simulated models of nanoparticle distributions in tumor tissue, we show that the time delay after which nanoparticle binding should be initiated is generalizable to a large variety of nanoparticle formulations and tumor scenarios. Recent advances in nanoparticle shielding technology provide evidence that such a strategy could be implemented in reality. In the future, we aim to further control the spatial distribution of nanoparticles in tissue based on local signals in the environment.

Acknowledgments

The authors are grateful to Dr. Fleming for her help in reviewing this manuscript. Dr. Hauert and Dr. Bhatia acknowledge support from the Human Frontier Science Program, The Marie-D. & Pierre Casimir-Lambert Fund, and NIH grant # U54 CA151884. Dr. Berman acknowledges support from National Science Foundation Expeditions in Computing grant CCF-0926148. Dr. Bhatia is an HHMI investigator. The authors wish to dedicate this paper to the memory of Officer Sean Collier for his caring service to the MIT community and for his sacrifice.

References

1. Nie S, Xing Y, Kim GJ, Simons JW. Annu Rev Biomed Eng. 2007; 9:257–288. [PubMed: 17439359]
2. Maeda H, Nakamura H, Fang J. Adv Drug Delivery Rev. 2012; 65:71–79.
3. Bao G, Mitragotri S, Tong S. Annu Rev Biomed Eng. 2013; 15:253–282. [PubMed: 23642243]
4. Jain RK, Stylianopoulos T. Nat Rev Clin Oncol. 2010; 7:653–664. [PubMed: 20838415]
5. Nichols JW, Bae YH. Nano Today. 2012; 7:606–618. [PubMed: 23243460]
6. Thurber GM, Wittrup KD. Cancer Res. 2008; 68:3334–3341. [PubMed: 18451160]
7. Lee H, Fonge H, Hoang B, Reilly RM, Allen C. Mol Pharm. 2010; 7:1195–1208. [PubMed: 20476759]
8. Cheng Z, Zaki AA, Hui JZ, Muzykantov VR, Tsourkas A. Science. 2012; 338:903–910. [PubMed: 23161990]
9. Rodriguez PL, Harada T, Christian DA, Pantano DA, Tsai RK, Discher DE. Science. 2013; 339:971–975. [PubMed: 23430657]
10. Ren Y, Cheung HW, von Maltzhan G, Agrawal A, Cowley GS, Weir BA, et al. Sci Transl Med. 2012; 4:147ra112.
11. Ren Y, Hauert S, Lo JH, Bhatia SN. ACS Nano. 2012; 6:8620–8631. [PubMed: 22909216]
12. Thurber GM, Weissleder R. PLoS ONE. 2011; 6:e24696. [PubMed: 21935441]
13. Wittrup KD, Thurber GM, Schmidt MM, Rhoden JJ. Methods Enzymol. 2012; 503:255–268. [PubMed: 22230572]
14. Decuzzi P, Ferrari M. Biomaterials. 2008; 29:377–384. [PubMed: 17936897]
15. Heldin CH, Rubin K, Pietras K, Ostman A. Nat Rev Cancer. 2004; 4:806–813. [PubMed: 15510161]
16. Lauffenburger, DA.; Linderman, J. Receptors: Models for Binding, Trafficking, and Signaling. Oxford University Press; New York: 1996.
17. Gardiner, C. Stochastic Methods: A Handbook for the Natural and Social Sciences. Springer; Berlin: 2009.
18. Nicolis, G.; Prigogine, I. Self-Organization in Nonequilibrium Systems: From Dissipative Structures to Order through Fluctuations. John Wiley & Sons; New York: 1977.
19. van Kampen, NG. Stochastic Processes in Physics and Chemistry. 2. Elsevier; Amsterdam: 1997.

20. Gillespie DT. J Comput Phys. 1976; 22:403–434.
21. Burrage, K.; Burrage, PM.; Leier, A.; Marquez-Lago, T.; Nicolau, DVJ. Design and Analysis of Biomolecular Circuits. Koeppl, H.; Setti, G.; di Bernardo, M.; Densmore, D., editors. Springer; New York: 2011. p. 43-62.
22. Lis M, Artyomov MN, Devadas S, Chakraborty AK. Bioinformatics. 2009; 25:2289–2291. [PubMed: 19578038]
23. Wong C, Stylianopoulos T, Cui J, Martin J, Chauhan VP, Jiang W, et al. Proc Natl Acad Sci USA. 2011; 108:2426–2431. [PubMed: 21245339]
24. Perrault SD, Walkey C, Jennings T, Fischer HC, Chan WCW. Nano Lett. 2009; 9:1909–1915. [PubMed: 19344179]
25. Hong S, Leroueil PR, Majoros IJ, Orr BG, Baker JR, Banaszak Holl MM. Chem Biol. 2007; 14:107–115. [PubMed: 17254956]
26. Tassa C, Duffner JL, Lewis TA, Weissleder R, Schreiber SL, Koehler AN, et al. Bioconjugate Chem. 2010; 21:14–19.
27. Choi CHJ, Alabi CA, Webster P, Davis ME. Proc Natl Acad Sci USA. 2010; 107:1235–1240. [PubMed: 20080552]
28. Cressman S, Dobson I, Lee JB, Tam YY, Cullis PR. Bioconjug Chem. 2009; 20:1404–1411. [PubMed: 19534457]
29. Zhou Y, Drummond DC, Zou H, Hayes ME, Adams GP, Kirpotin DB, et al. J Mol Biol. 2007; 371:934–947. [PubMed: 17602702]
30. Jiang W, Kim BYS, Rutka JT, Chan WCW. Nat Nanotechnol. 2008; 3:145–150. [PubMed: 18654486]
31. Poon Z, Chen S, Engler AC, Li H, Atas E, von Maltzahn G, et al. Angew Chem. 2010; 49:7266–7270. [PubMed: 20740515]
32. Doiron AL, Clark B, Rinker KD. Biotechnol Bioeng. 2011; 108:2988–2998. [PubMed: 21766288]
33. Sutherland W. Philos Mag. 1905; 9:781–785.
34. Sailor MJ, Park JH. Adv Mater. 2012; 24:3779–3802. [PubMed: 22610698]
35. Artemov D, Mori N, Okollie B, Bhujwalla ZM. Magn Reson Med. 2003; 49:403–408. [PubMed: 12594741]
36. Bae Y, Park K. J Controlled Release. 2011; 153:198–205.
37. Dreaden EC, Austin LA, Mackey MA, El-Sayed MA. Ther Deliv. 2012; 3:457–478. [PubMed: 22834077]
38. Hainfeld JF, O'Connor MJ, Dilmanian FA, Slatkin DN, Adams DJ, Smilowitz HM. Brit J Radiol. 2011; 84:526–533. [PubMed: 21081567]
39. Gabizon A, Shmeeda H, Grenader T. Eur J Pharm Sci. 2012; 45:388–398. [PubMed: 21933707]
40. Reagan-Shaw S, Nihal M, Ahmad N. FASEB J. 2008; 22:659–661. [PubMed: 17942826]
41. Parr MJ, Masin D, Cullis PR, Bally MB. J Pharmacol Exp Ther. 1997; 280:1319–1327. [PubMed: 9067319]
42. Mammen M, Choi SK, Whitesides GM. Angew Chem. 1998; 37:2754–2794.
43. Allen TM, Cullis PR. Adv Drug Delivery Rev. 2013; 65:36–48.
44. Heath TD, Fraley RT, Bentz J, Voss EW, Herron JN, Papahadjopoulos D. Biochim Biophys Acta. 1984; 770:148–158. [PubMed: 6421325]
45. Gao H, Yang Z, Zhang S, Cao S, Shen S, Pang Z, et al. Sci Rep. 2013; 3:2534. [PubMed: 23982586]
46. Igawa T, Ishii S, Tachibana T, Maeda A, Higuchi Y, Shimaoka S, et al. Nat Biotechnol. 2010; 28:1203–1207. [PubMed: 20953198]
47. Albanese A, Tang PS, Chan WCW. Annu Rev Biomed Eng. 2012
48. Thurber GM, Figueiredo JL, Weissleder R. PLoS ONE. 2009; 4:e8053. [PubMed: 19956597]
49. Kim CS, Duncan B, Creran B, Rotello VM. Nano Today. 2013 in press.
50. Poon Z, Chang D, Zhao X, Hammond PT. ACS Nano. 2011; 5:4284–4292. [PubMed: 21513353]
51. Hatakeyama H, Akita H, Kogure K, Oishi M, Nagasaki Y, Kihira Y, et al. Gene Ther. 2007; 14:68–77. [PubMed: 16915290]

52. Harris TJ, von Maltzahn G, Lord ME, Park JH, Agrawal A, Min DH, et al. Small. 2008; 4:1307–1312. [PubMed: 18690639]
53. Harris TJ, von Maltzahn G, Derfus AM, Ruoslahti E, Bhatia SN. Angew Chem. 2006; 45:3161–3165. [PubMed: 16642514]
54. Lee ES, Gao Z, Kim D, Park K, Kwon IC, Bae YH. J Controlled Release. 2008; 129:228–236.
55. Kairdolf BA, Nie S. J Am Chem Soc. 2011; 133:7268–7271. [PubMed: 21510704]
56. von Maltzahn G, Park JH, Lin KY, Singh N, Schwöppe C, Mesters R, et al. Nat Mater. 2011; 10:545–552. [PubMed: 21685903]
57. Olson ES, Aguilera TA, Jiang T, Ellies LG, Nguyen QT, Wong EH, et al. Integr Biol. 2009; 1:382–393.
58. Olson ES, Jiang T, Aguilera TA, Nguyen QT, Ellies LG, Scadeng M, et al. Proc Natl Acad Sci USA. 2010; 107:4311–4316. [PubMed: 20160077]
59. Nguyen QT, Olson ES, Aguilera TA, Jiang T, Scadeng M, Ellies LG, et al. Proc Natl Acad Sci USA. 2010; 107:4317–4322. [PubMed: 20160097]
60. Crayton S, Tsourkas A. ACS Nano. 2012; 5:9592–9601. [PubMed: 22035454]
61. Romberg B, Hennink WE, Storm G. Pharm Res. 2008; 25:55–71. [PubMed: 17551809]
62. Lee SE, Liu GL, Kim F, Lee LP. Nano Lett. 2009; 9:562–570. [PubMed: 19128006]
63. Partlow KC, Lanza GM, Wickline SA. Biomaterials. 2008; 29:3367–3375. [PubMed: 18485474]

Biographies

Sabine Hauert is a Human Frontier Science Program Cross-Disciplinary Fellow at the Koch Institute for Integrative Cancer Research at MIT. She aims to engineer swarming nanosystems for the treatment of diseases using novel computational tools such as machine learning and crowdsourcing. She completed her M.Sc. in Computer Science and Ph.D. at EPFL in Switzerland where she worked on controlling swarms of flying robots.

Spring Berman is an assistant professor of Mechanical and Aerospace Engineering at Arizona State University. She received the B.S.E. degree in Mechanical and Aerospace Engineering from Princeton University in 2005 and the M.S.E. and Ph.D. degrees in Mechanical Engineering and Applied Mechanics from the University of Pennsylvania in

2008 and 2010, respectively. From 2010 to 2012, she was a postdoctoral researcher in Computer Science at Harvard University. Her research focuses on the modeling, simulation, and analysis of behaviors in both biological and engineered collectives and the synthesis and optimization of control strategies for multi-robot systems, including robotic swarms.

Radhika Nagpal is professor in Computer Science, in the Harvard School of Engineering and Applied Sciences and core faculty member of the Wyss Institute for Biologically Inspired Engineering, where she co-lead the BioRobotics Platform. She is also affiliated with the Department of Systems Biology at Harvard Medical School. She was a graduate student and postdoc lecturer at the MIT CSAIL, a member of the Amorphous Computing Group and a Bell Labs GRPW graduate fellow. She received the Microsoft New Faculty Fellowship Award, NSF Career Award, the Thomas D. Cabot Associate Professor Chair, the Borg Early Career Award, and a Radcliffe Fellowship.

Sangeeta N. Bhatia is the John J. and Dorothy Wilson Professor of Health Sciences and Technology and Electrical Engineering and Computer Science at MIT and a Howard Hughes Medical Investigator. Her lab combines engineering and biology to develop micro- and nanoscale platforms for understanding, and treating human disease. Dr. Bhatia received her B.S. from Brown University, M.S. and Ph.D. from MIT, M.D. from Harvard and completed graduate and post-doctoral training at MGH. Prior to MIT, Dr. Bhatia held a faculty position at UCSD, and worked at Pfizer, Genetics Institute, ICI Pharmaceuticals, and Organogenesis. Dr. Bhatia has published >100 manuscripts and over 40 issued or pending patents, and has co-founded two biotechnology start-ups, consults for industry, government and academic organizations, and advocates for diversity in science and engineering.

Highlights

- Binding and diffusion affect the penetration of targeted nanoparticles in tumors.
- Simulations show many nanoparticle formulations accumulate in cells near vessels.
- Shielding prevents nanoparticles from binding until they diffuse deep in tissue.
- Shielding strategy is generalizable to many nanoparticles and tumor scenarios.
- Time or space-dependent binding enables engineered nanoparticle tissue distributions.

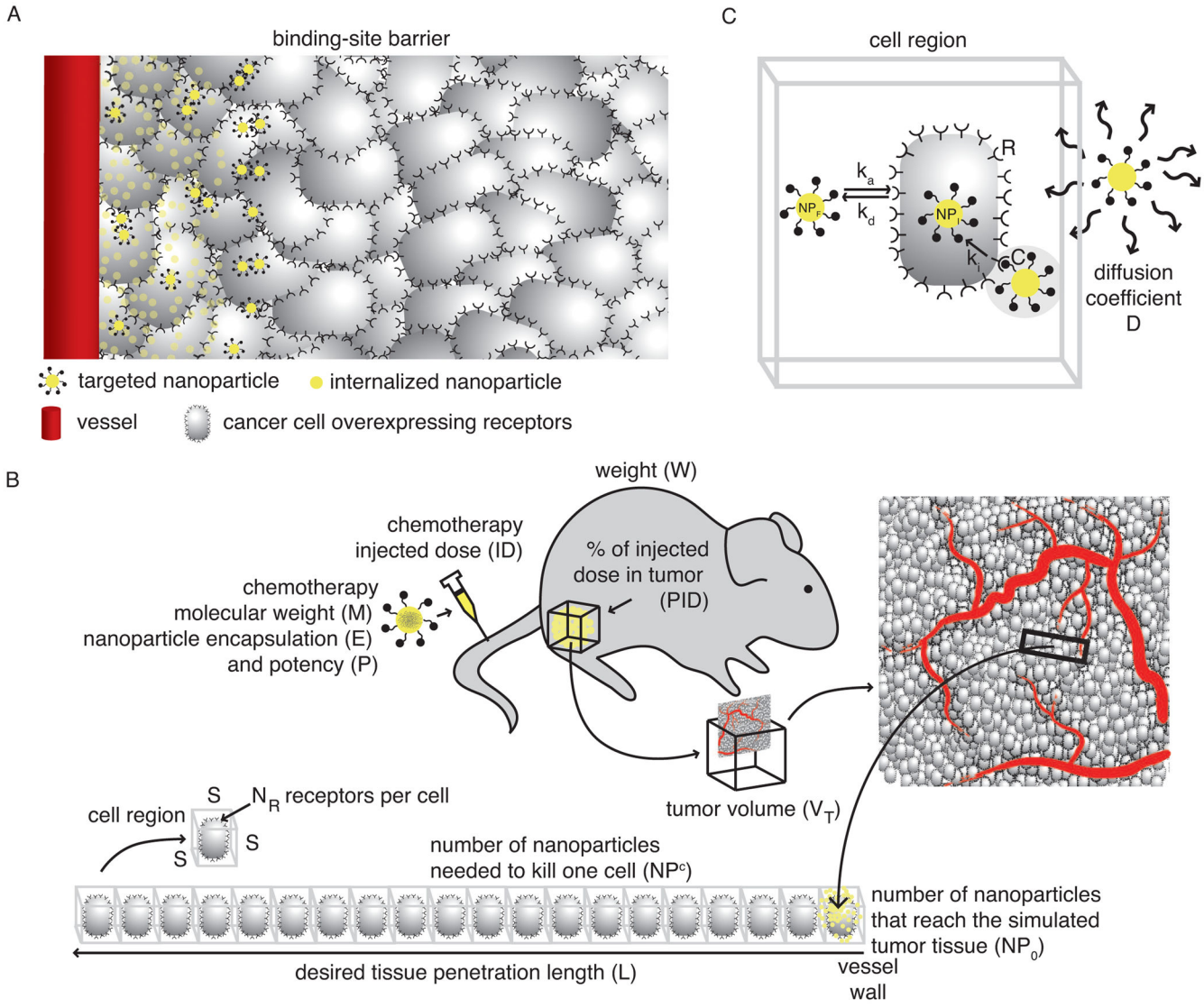

Fig. 1. Model used to simulate tissue penetration and cellular accumulation of targeted nanoparticles

A) Targeted nanoparticles are at risk of accumulating mostly in cells close to the vasculature, leading to binding-site barriers. B) Parameters used to determine the number of injected nanoparticles that will reach the simulated tumor section. The tissue section model represents a challenging scenario in which nanoparticles leaving vessels near the necrotic core of the tumor need to penetrate deep into tumor tissue. C) Reaction-diffusion model used to simulate the diffusion, binding kinetics, and cellular internalization of targeted nanoparticles in tumor tissue. Free nanoparticles diffuse throughout the tissue with diffusion coefficient *D*. The species in the reaction network are defined as NP_F, free nanoparticles; NP_I, internalized nanoparticles; *R*, receptors; and *C*, nanoparticle-receptor complexes. *ka* and *kd* are the association and dissociation rate constants and *ki* is the internalization rate constant.

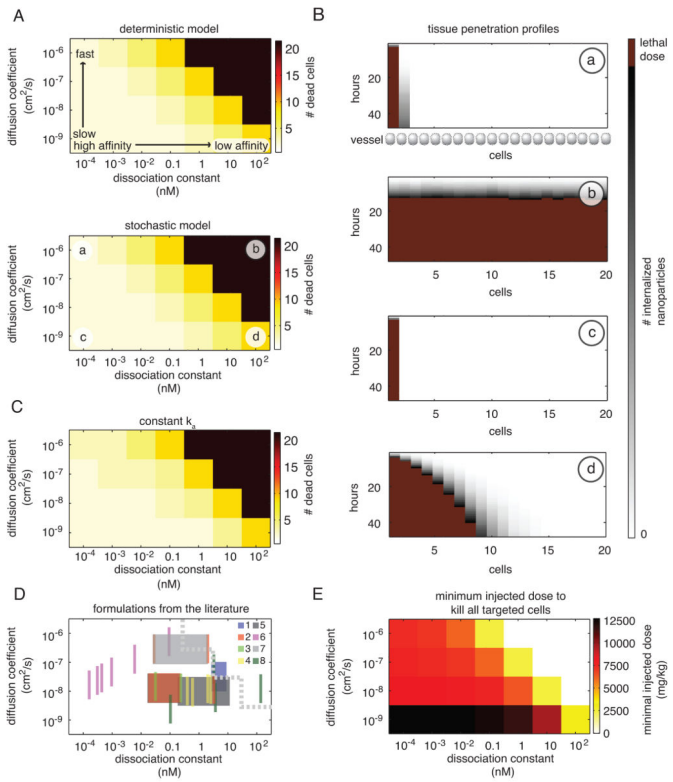

Fig. 2. Identification of binding-site barriers

A) Number of cells killed depending on the nanoparticle formulation (i.e., diffusion coefficient D and dissociation constant $K_D = k_d/k_a$) with k_d fixed and k_a varying. Complete tissue penetration is assumed when each of the 20 cells in the model internalizes the number of nanoparticles required to kill one cell (estimated lethal cell dose), which for this scenario is over 600 nanoparticles. Results obtained using the deterministic model are validated using a stochastic simulator. B) Tissue penetration profiles determined using a stochastic simulator for four combinations of the diffusion coefficients and dissociation constants labeled in Fig. 2A. C) Number of cells killed depending on the nanoparticle formulation with k_a fixed and k_d varying ($K_D = k_d/k_a$). D) Representative nanoparticle formulations identified in the literature (Table 1). Diffusion coefficients were calculated based on nanoparticle radii and viscosities ranging from values for water to values for tumor tissue rich in collagen fiber [4]. Many formulations in the literature would perform poorly in our test scenario due to binding-site barriers, which occur for each parameter set (K_D, D) below the dashed line. E) Minimum injected dose of chemotherapy required to theoretically kill all cells in the simulated scenario for each nanoparticle formulation. Resulting high doses could cause systemic toxicity in mice [41].

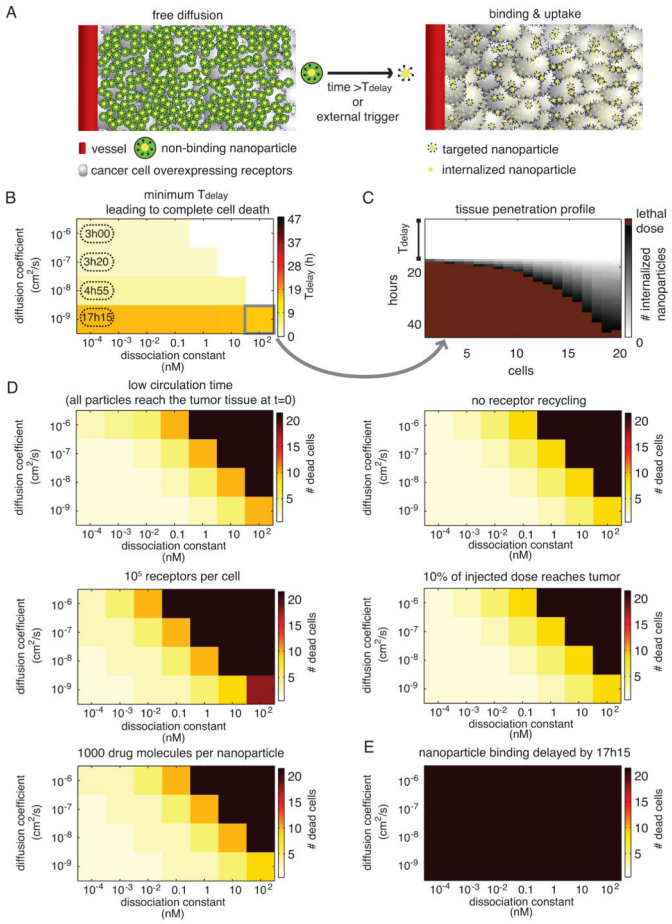

Fig. 3. Time-dependent binding strategy for targeted deep tissue penetration

A) The delayed binding strategy allows nanoparticles to diffuse deep into the tissue before unveiling their targeting moieties as a function of time or an external trigger. B) Minimum binding delays leading to the death of all target cells for each nanoparticle formulation. For each diffusion rate, we note the minimum T_{delay} value that would result in death of all target cells across each dissociaiton constant (dashed lines). C) Stochastic simulation of the delayed binding strategy for a nanoparticle formulation with the T_{delay} value indicated in Fig. 3B. The delay in binding can clearly be seen by the lack of internalization during the first hours of the simulation. A lethal dose in a cell is reached when the cell accumulates over 600 nanoparticles. D) Impact of the scenario on the prevalence of binding-site barriers, as predicted by the deterministic model. Each simulated scenario uses an injected dose of 33 mg/kg, does not implement a binding delay, and varies one of the following parameters: nanoparticle circulation time, receptor recycling, receptor expression, nanoparticle accumulation in the tumor, and drug loading. Binding-site barriers arise in all scenarios. E) Delaying binding by 17h15 for all nanoparticle formulations leads to death of all target cells in all scenarios without changing the injected dose of 33 mg/kg, thereby demonstrating the generalization of our guidelines to a large number of tumor environments.

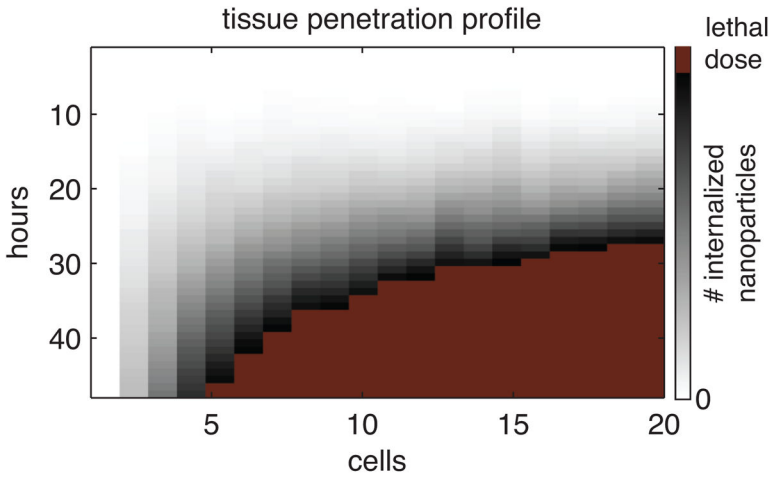

Fig. 4. Space-dependent binding strategy for targeted deep tissue penetration

Nanoparticles are engineered to unshield targeting moieties as a function of their environment. The stochastic simulator was used to obtain a tissue penetration profile for nanoparticles engineered to accumulate most in cells far away from the vasculature; such inverted internalization gradients could help deliver drugs deep into tumors.

Table 1

Nanoparticle radii and dissociation constants reported in the literature.

#	*r* [nm]	K_D [nM]	Scenario	Ref
1	38	2.84 – 9.08	Iron oxide nanoparticles targeted to FKBP12	[26]
2	4	0.03 – 2.00	Dendrimer-based nanodevices targeted to folate receptors	[25]
3	81, 87	0.03, 0.23	Gold nanoparticles targeted to human transferrin	[27]
4	94.2, 102.2, 128.9, 117.4	1.98, 2.59, 0.59, 0.38	Liposomal nanoparticles targeted to RGD	[28]
5	120	0.18 – 11.76	Liposomes targeted to EGFR	[29]
6	2, 10, 25, 40, 50, 70	0.09, 0.005, 0.0009, 0.0004, 0.0003, 0.00015	Gold nanoparticles targeted to ErbB2	[30]
7	90	0.017, 0.04, 0.092, 0.15, 0.2, 3.1, 3.3	Patchy micelles targeted to folate receptors	[31]
8	20, 100, 200, 500	142, 3.83, 0.097, 0.026	Polystyrene nanoparticles targeted to endothelial cells	[32]

Table 2

Parameter values for the simulation test-case scenario.

S	largest cell dimension	10 μm
N_R	number of receptors per cell	10^6
W	animal weight	20 g
ID	injected dose of doxorubicin	33 mg/kg
PID	percentage of injected dose in tumor	1%
E	number of molecules of doxorubicin per particle	10^4
P	IC90 of doxorubicin	10 μM
M	molar mass of doxorubicin	543.52 g/mol
V_T	tumor volume	5 mm × 5 mm × 5 mm
L	desired tissue penetration depth	200 μm
T	time at which PID is measured	48 hours
T_C	circulation time of the nanoparticles	24 hours